NEURAL REGENERATION RESEARCH
January 2016, Volume 11, Issue 1
www.nrronline.org

RESEARCH ARTICLE

Angiogenesis in tissue-engineered nerves evaluated objectively using MICROFIL perfusion and micro-CT scanning

Hong-kui Wang[1, 2, #], Ya-xian Wang[2, #], Cheng-bin Xue[2], Zhen-mei-yu Li[2], Jing Huang[2], Ya-hong Zhao[2], Yu-min Yang[2], Xiao-song Gu[1, 2, *]

1 School of Biology and Basic Medical Sciences, Soochow University, Suzhou, Jiangsu Province, China
2 Jiangsu Key Laboratory of Neuroregeneration, Nantong University, Nantong, Jiangsu Province, China

How to cite this article: *Wang HK, Wang YX, Xue CB, Li ZMY, Huang J, Zhao YH, Yang YM, Gu XS (2016) Angiogenesis in tissue-engineered nerves evaluated objectively using MICROFIL perfusion and micro-CT scanning. Neural Regen Res 11(1):168-173.*

Funding: *This study was supported by the National Natural Science Foundation of China, No. 81130080.*

Graphical Abstract

MICROFIL perfusion and micro-CT scanning is a good method for visualizing newly formed blood vessels in tissue-engineered nerves implanted *in vivo*

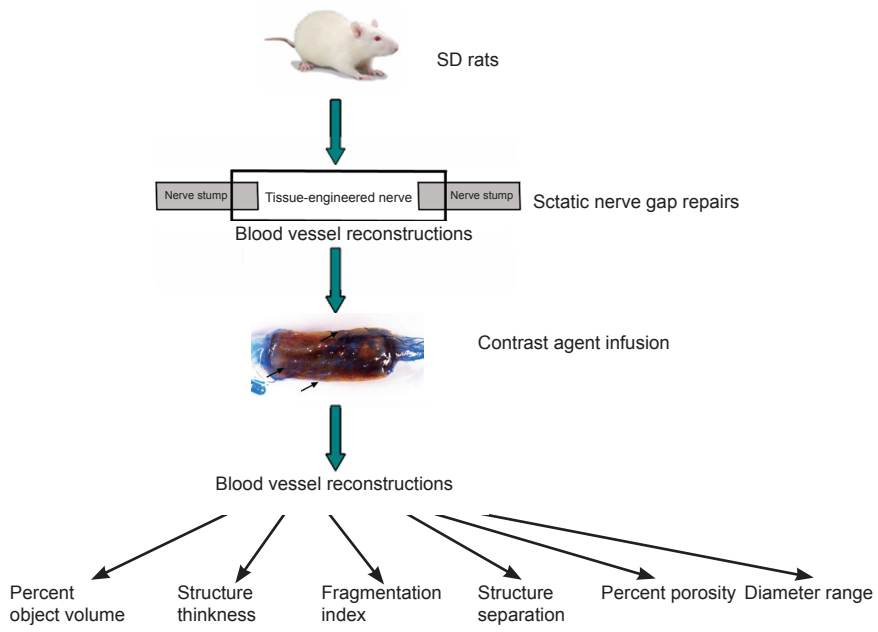

***Correspondence to:**
Xiao-song Gu, M.D., nervegu@ntu.edu.cn.

 # These authors contributed equally to this work.

orcid:
0000-0002-2562-6275 (Xiao-song Gu)

doi: *10.4103/1673-5374.175065*
http:*//www.nrronline.org/*

Accepted: *2015-09-23*

Abstract

Angiogenesis is a key process in regenerative medicine generally, as well as in the specific field of nerve regeneration. However, no convenient and objective method for evaluating the angiogenesis of tissue-engineered nerves has been reported. In this study, tissue-engineered nerves were constructed *in vitro* using Schwann cells differentiated from rat skin-derived precursors as supporting cells and chitosan nerve conduits combined with silk fibroin fibers as scaffolds to bridge 10-mm sciatic nerve defects in rats. Four weeks after surgery, three-dimensional blood vessel reconstructions were made through MICROFIL perfusion and micro-CT scanning, and parameter analysis of the tissue-engineered nerves was performed. New blood vessels grew into the tissue-engineered nerves from three main directions: the proximal end, the distal end, and the middle. The parameter analysis of the three-dimensional blood vessel images yielded several parameters, including the number, diameter, connection, and spatial distribution of blood vessels. The new blood vessels were mainly capillaries and microvessels, with diameters ranging from 9 to 301 μm. The blood vessels with diameters from 27 to 155 μm accounted for 82.84% of the new vessels. The microvessels in the tissue-engineered nerves implanted *in vivo* were relatively well-identified using the MICROFIL perfusion and micro-CT scanning method, which allows the evaluation and comparison of differences and changes of angiogenesis in tissue-engineered nerves implanted *in vivo*.

Key Words: *nerve regeneration; angiogenesis; micro-CT; MICROFIL perfusion; three-dimensional reconstruction; tissue-engineered nerve; skin-derived precursor; chitosan nerve conduit; Schwann cell; neural regeneration*

Introduction

Blood vessels, which are spread throughout the body providing oxygen and nutrients and removing metabolites, are an important support system (Carmeliet and Jain, 2011; Potente et al., 2011). Encouraging faster and more efficient angiogenesis in regenerative tissues and organs can improve their survival and physiological functions, making them better physiological substitutes (Goerke et al., 2015; Jiang et al., 2015). In the fields of regenerative medicine and regenerative tissue engineering, the focus of research has increasingly been on establishing a blood supply for the regenerated tissues and organs (Dew et al., 2015; Osborn et al., 2015; Shafiq et al., 2015; Unger et al., 2015), which is one critical bottleneck in regenerative medicine.

Our group has focuses on the research and exploration of peripheral nerve tissue regeneration (Wang et al., 2005, 2012, 2014b; Hu et al., 2013; Gu et al., 2014; Li et al., 2015; Zhou et al., 2015) because of the critical importance of angiogenesis in tissue-engineered nerves. Blood vessels can be encouraged to grow into chitosan nerve conduits, the basis of creating tissue-engineered nerves, through the innovative use of certain key technologies. However, the objective and comprehensive imaging and evaluation of neovascularization in tissue-engineered nerves remain technical problems. In the present study, we report a better method for evaluating angiogenesis in tissue-engineered nerves. Three-dimensional reconstruction of the blood vessels in implanted tissue-engineered nerves is difficult because the microvessels are denser and thinner than those found in normal spinal cords and sciatic nerves. As a contrast agent, the MICROFIL complex has several advantages such as allowing better imaging of the microvessels, better filing, and less shrinkage after curing than other contrast agents.

The three-dimensional reconstruction of blood vessels in tissue-engineered nerves bridging 10-mm sciatic nerve defects was observed in the present study for the first time using MICROFIL perfusion and micro-CT scanning. This method provided relevant data on the reconstructed blood vessels for understanding the mechanisms underlying angiogenesis and elevating the angiogenesis in tissue-engineered nerves.

Materials and Methods

Fabrication of chitosan nerve conduits

Chitosan (Nantong Xincheng Biochemical Company, Nantong, Jiangsu Province, China) was purified twice through dissolution in 10 g of acetic acid, filtration, precipitation with 50 g of NaOH, and finally drying in a vacuum at room temperature. The degree of chitosan deacetylation was 92.3%, as measured by titration. After 5 g of chitosan had completely dissolved in 100 mL of 0.15 M hydrochloric acid, 10% gelatin was added, followed by 5 g of chitin powder, with stirring to form an opaque viscous liquid. The chitin/chitosan mixture was then injected into stainless-steel casting molds, which were then sealed and placed at −12°C for 2–4 hours. Next, the frozen gels were removed and soaked in 4 M NaOH for 4 hours to neutralize any remaining lactic acid and to complete the solidification. The conduits were then rinsed repeatedly with distilled water to remove any residual NaOH and sodium lactate and lyophilized under a 35–45 mTorr vacuum for 20 hours. The resulting porous conduits were 2 mm inner diameter, 3 mm outer diameter, and 80 mm long (Yang et al., 2011).

Ethics statement

All experimental protocols were approved by the Administration Committee of Experimental Animals, Jiangsu Province, China, in accordance with the guidelines of the Institutional Animal Care and Use Committee, Nantong University, China. Institutional Animal Care and Use Committee approval was obtained before beginning the animal studies. Every effort was made to minimize suffering and the number of animals used in each experiment.

Construction of tissue-engineered nerves

Tissue-engineered nerves were constructed *in vitro* using Schwann cells differentiated from rat skin-derived precursors (SKPs) (SKP-SCs) as supporting cells and chitosan nerve conduits combined with silk fibroin fibers as scaffolds in a rotary perfusion cell culture (Rotary Culture MW^{TM}) bioreactor (Synthecon, Inc, Houston, TX, USA).

A clean 1-day-old female Sprague-Dawley rat was provided by the Experimental Animal Center of Nantong University, China (license No. SCXK (Su) 2008-0010). Briefly, approximately 2 cm^2 of dorsal skin was dissociated. The SKPs from this newborn Sprague-Dawley rat were isolated, cultured, induced to differentiate into SKP-SCs directly, and expanded *in vitro* (Toma et al., 2001; Biernaskie et al., 2006). The suspension of SKP-SCs and scaffolds were placed in the rotary culture container filled with complete medium, which was cultured in an incubator at 37°C, 5% CO_2, and rotational speed of 10 r/min to provide sufficient contact between the cells and scaffolds. The final cell density was 10^6 cells/mL. To allow scaffold suspension in the culture liquid, the rotational speed of the microgravity bioreactor was adjusted 24 hours after cell attachment. The tissue-engineered nerves were stored in normal saline after rinsing twice with normal saline.

Establishment of the sciatic nerve injury model

Three female, 2-month-old clean Sprague-Dawley rats were provided by the Experimental Animal Center of Nantong University, China (license No. SCXK (Su) 2008-0010). The animals were housed in a temperature-controlled environment and allowed free access to food and water. First, the rats were deeply anesthetized with an intraperitoneal injection of a compound anesthetic (chloral hydrate 4.25 g, magnesium sulfate 2.12 g, sodium pentobarbital 886 mg, ethanol 14.25 mL, and propylene glycol 33.8 mL in 100 mL) at a dose of 0.2–0.3 mL/100 g. An incision through the skin and muscle was made to expose the sciatic nerve at the

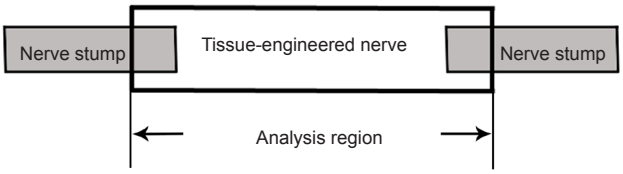

Figure 1 Schematic diagram of the analysis region.
The main portion of each tissue-engineered nerve (the part between the arrows) was selected for parameter analysis. The nerve stumps at the ends of the tissue-engineered nerves were excluded.

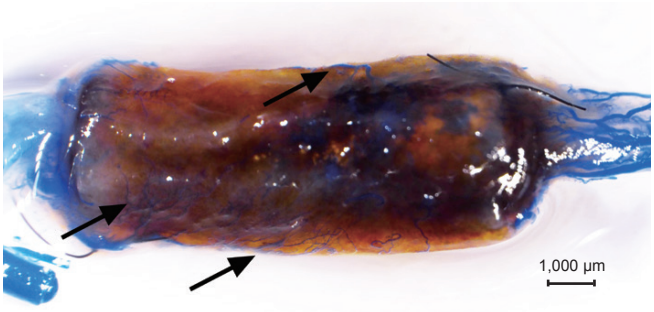

Figure 2 Tissue-engineered nerve after clearing with glycerin.
The proximal end is on the right, and the distal end on the left. The nerve stumps at the ends of the tissue-engineered nerves and connective tissues surrounding the tissue-engineered nerves were transparent. The chitosan nerve conduits appeared semitransparent. Both the small vessels in the nerve stumps and the microvessels growing into the tissue-engineered nerves were filled with blue contrast agent (arrows) and are clearly visible. The microvessels growing into the tissue-engineered nerves from the surrounding tissues are indicated with arrows.

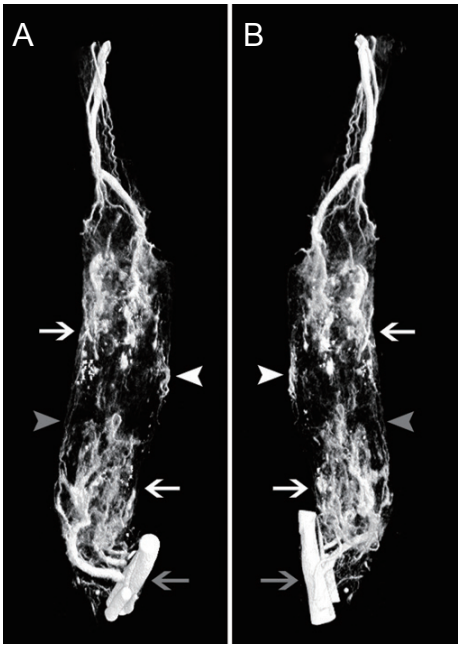

Figure 3 Three-dimensional reconstructions of blood vessels in tissue-engineered nerve.
(A, B) Views from two different angles of a three-dimensional reconstruction. The proximal end is at the top, and the distal end at the bottom. The blood vessels of the popliteal fossa are indicated by the gray arrow. A large number of microvessels and capillaries were relatively well visualized. Microvessels growing into the tissue-engineered nerves are indicated with white arrows. New blood vessels grew into the tissue-engineered nerves from three main directions: the proximal end, the distal end, and the middle. The microvessels growing in from the middle part are indicated with white arrowheads. The microvessels connecting the proximal and distal ends are indicated with gray arrowheads.

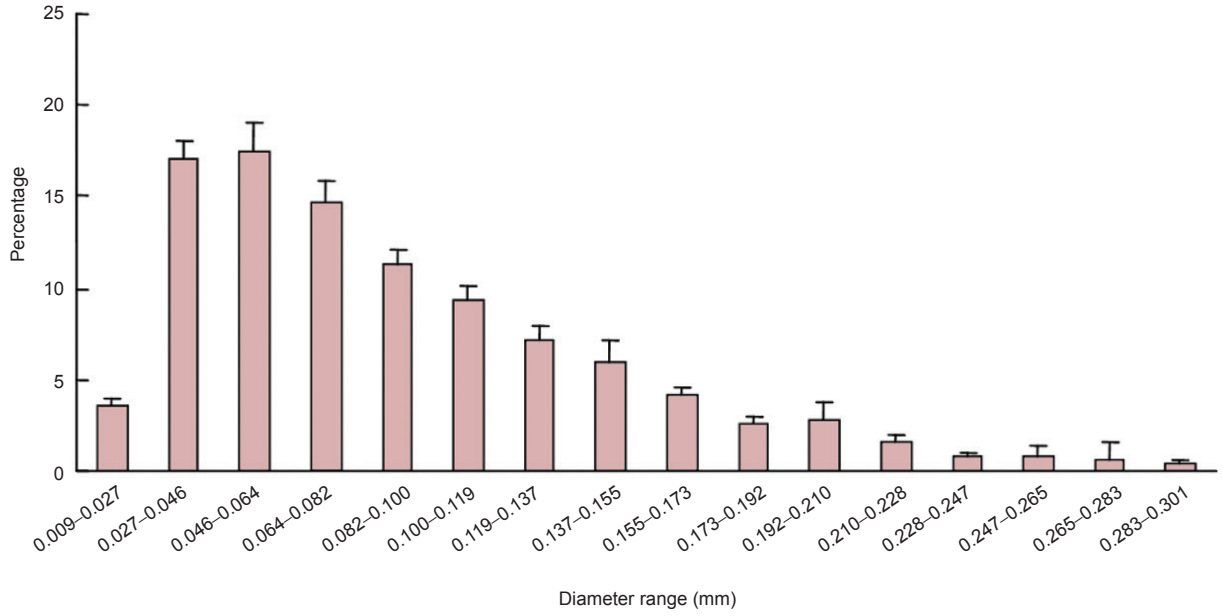

Figure 4 Blood vessel diameter distribution based on the three-dimensional reconstructions of the blood vessels in the tissue-engineered nerves.
The data are presented as the mean ± SD based on the three rats analyzed in this study. The new blood vessels were mainly capillaries and microvessels with diameters ranging from 9 to 301 μm. Blood vessels with diameters of 27 to 155 μm accounted for 82.84% of all vessels.

Table 1 Parameters from the three-dimensional reconstructions of the blood vessels

Parameter	1	2	3	mean±SD
Percent object volume (%)	3.91	1.96	4.48	3.45±1.32
Structure thickness (mm)	0.09	0.10	0.09	0.09±0.01
Fragmentation index (1/mm)	21.78	39.86	30.88	30.84±9.04
Structure separation (mm)	0.86	0.76	0.44	0.69±0.22
Percent porosity (%)	0.22	0.09	0.12	0.15±0.07

1, 2, and 3: Different individual animals. Percent object volume (%): the number of blood vessels per volume. Structure thickness (mm): the diameter of the blood vessels. Fragmentation index (1/mm): the connection of the blood vessels. Structure separation (mm) and percent porosity (%): the spatial distribution of the blood vessels.

left mid-thigh. An 8-mm section of the sciatic nerve (from approximately 10 mm distal to the proximal end to the ischial tuberosity) was resected to produce a 10-mm gap after slight retraction of the distal and proximal stumps. A tissue-engineered nerve was implanted to bridge the gap, and the proximal and distal nerve stumps were each inserted 1 mm into either end of the conduit. Then, the muscle layers and skin were sutured closed in layers. After the surgery, the animals recovered in warm cages (Yang et al., 2011).

Perfusion of contrast agents

Four weeks after surgery, the rats were again deeply anesthetized with the compound anesthetic. Each animal was infused with approximately 500 mL of normal saline mixed with 0.8 mL heparin sodium to a final concentration of 10 U/mL (Changzhou Qianhong Pharmaceutical Co., Ltd., Changzhou, Jiangsu Province, China) through a pinhead inserted into the left ventricle. Then, a blue-colored (MV-120) MICROFIL compound (MV 20 mL, diluent 25 mL, and curing agent 2.25 mL) (Flow Tech, Inc., Carver, MA, USA) was infused into the aorta with a 5-mL syringe. The perfusion was continued until the contrast agent outflow was observed from the right atrium and part of the liver turned blue. The perfusion pressure was approximately 100 cmH_2O. The volume of contrast agents infused was approximately 40 mL. The working time of the MICROFIL compounds was 20 minutes from the addition of the curing agent to the other compounds. Finally, the root of the aorta was ligated with surgical sutures, and the rat was placed in a refrigerator at 4°C overnight to allow the contrast agents to cure.

Collection and treatment of samples

After the contrast agents had cured, the surgical site at the left mid-thigh was reopened to expose the tissue-engineered nerve. Then, the tissue-engineered nerve and nerve ends were harvested and cleared in glycerin. Each sample was placed in a 50% mixture of water and glycerin. At successive 24-hour intervals, the glycerin concentration was raised to 75%, 85%, and finally 100%. This procedure cleared the tissue to allow the microscopic examination to select a well-perfused region of the blood vessels for micro-CT scanning.

Scanning, parameter analysis, and three-dimensional reconstruction of blood vessels by micro-CT

The samples were scanned in a SkyScan1076 micro-CT (Bruker Corporation, Billerica, MA, USA) at 29 kV voltage, 169 μA current, and 8.8 μm resolution. Each sample took approximately 14 minutes to scan. Three-dimensional images of the blood vessels were reconstructed. The SkyScan CTVOX 2.1 software was used to automatically quantify several parameters, including percent object volume (%), structure thickness (mm), fragmentation index (1/mm), structure separation (mm), and percent porosity (%). Most of each tissue-engineered nerve was used when analyzing the parameters, but the nerve stumps at the ends of the tissue-engineered nerves were excluded (**Figure 1**).

Statistical analysis

The data are presented as the mean ± SD. The data were calculated and analyzed using the Stata 7.0 software package (Stata Corp., College Station, TX, USA).

Results

General appearance of the tissue-engineered nerves

The tissue-engineered nerve samples, after perfusion of the contrast agent, became transparent through dehydration in the glycerin gradient. The nerve stumps at the ends of the tissue-engineered nerves and connective tissues surrounding the tissue-engineered nerves were transparent, while the chitosan nerve conduits appeared semitransparent. After clearing, the tissue-engineered nerve samples could be observed and imaged directly under the light microscope. The microvessels filled with blue contrast agent were clearly visible, which was helpful for checking the effect of perfusion on the blood vessels to facilitate better three-dimensional image reconstruction (**Figure 2**).

Three-dimensional reconstructions of the blood vessels in the tissue-engineered nerves

Three-dimensional reconstructions of the blood vessels that formed after the tissue-engineered nerves were implanted *in vivo* were acquired through micro-CT scanning and subsequent image processing after perfusion of the contrast agent (**Figure 3**). A large number of microvessels and capillaries were relatively well-visualized. New blood vessels had grown into the tissue-engineered nerves from three main directions: the proximal end, the distal end, and the middle, which is consistent with prior observations. In addition to the large number of visible microvessels growing into the tissue-engineered nerves, a few microvessels connecting the proximal and distal ends were also observed.

Parameter analysis of the three-dimensional blood vessel reconstructions

Quantitative parameter analysis was conducted on the three-dimensional reconstructions of the majority of the tissue-engineered nerves (**Figure 1**). The parameters identified the number, diameter, connection, and spatial distribution of the blood vessels (**Table 1**). By further analyzing the blood

vessel diameters, the proportion and distribution of neovascular diameters in the tissue-engineered nerves implanted *in vivo* were determined (**Figure 4**). The new blood vessels were mainly capillaries and microvessels, and their diameters ranged from 9 to 301 μm. Blood vessels with diameters from 27 to 155 μm accounted for 82.84% of the vessels.

Discussion

No convenient and objective method for evaluating angiogenesis in tissue-engineered nerves that includes three-dimensional information on the new blood vessels has been reported. However, several detailed reports have examined angiogenesis in tissue-engineered nerves. The results of the present study suggest that the method of MICROFIL perfusion and micro-CT scanning is well-suited for imaging and evaluating angiogenesis in tissue-engineered nerves.

Blood vessels can be visualized under the microscope using conventional or specialized staining of tissue sections, but these techniques cannot provide information on the spatial distribution of vessels (Jin et al., 2005; Oxlund et al., 2010; Marinković et al., 2013; Savransky et al., 2013; Wang et al., 2014a, c). Three-dimensional reconstructions of blood vessels can be obtained based on tissue sectioning and staining, but this approach takes a lot of time and effort and requires advanced tissue slicing technology. It is difficult to avoid the loss of objective information during tissue slicing. Blood vessels can also be visualized by perfusion. For example, resin and ink are common perfusion agents for visualizing vessels with large diameters because they fill the vessels incompletely and insufficiently. Furthermore, these agents do not allow direct scanning (Kanzaki et al., 1982; Cheung, 1996; Walter et al., 2012; Hasan et al., 2013; Xue et al., 2014).

Blood vessel three-dimensional reconstruction using MICROFIL perfusion and micro-CT scanning is convenient, feasible, and visualizes microvessels well (Garcia-Sanz et al., 1998; Nyangoga et al., 2011; Barbetta et al., 2012; Jing et al., 2012; Liu et al., 2013; Kline et al., 2014; Lee et al., 2014). The method contains two steps: blood vessel perfusion with the MICROFIL compounds, and micro-CT scanning of the tissue samples. Both stages are important for producing the best three-dimensional reconstructions of the blood vessels. The technical procedure and necessary precautions during blood vessel perfusion (*i.e.* the preparation of the tissue samples) are more detailed than the micro-CT scanning.

During perfusion, normal saline and contrast agents must be prevented from entering the pulmonary circulation or the microvessels will not be filled well because of insufficient pressure. The flow should be well-distributed and the pressure should be constant when the contrast agents are injected using a syringe. Too little pressure causes inadequate filling of the microvessels, while too large a pressure causes blood vessels to burst. In addition, air bubbles must be prevented from entering the blood vessels. The ligation of the root of the aorta must be performed immediately following the perfusion to prevent the contrast agents from flowing out before the contrast agent compounds have time to cure.

The selection of the voltage for micro-CT scanning should be decided while considering the number of microvessels, the amount of tissue surrounding the blood vessels, and the continuity of the vessels. The diameter of the thinnest capillary is approximately 10 μm. The spatial resolution of the micro-CT must be at least that size to image the smallest vessels. In addition to the above factors, the limitations of the MICROFIL contrast agent compounds and micro-CT themselves should also be considered. With the advancement of experimental technologies and instruments, three-dimensional imaging of blood vessels will become more and more sophisticated, objective, and accurate.

One significant advantage of this technique is that relevant quantitative data on the blood vessels (the number, diameter, connection, and spatial distribution) can be obtained from the three-dimensional reconstructions of the blood vessels in the tissue-engineered nerves using the parameter analysis software bundled with the scanning system. Thus, a more objective and comprehensive understanding of angiogenesis in tissue-engineered nerves implanted *in vivo* was acquired. The quantitative nature of the data allows us to objectively compare the differences and changes in angiogenesis in tissue-engineered nerves implanted *in vivo* under different conditions. This provides a better method and premise for exploring the factors that promote angiogenesis in tissue-engineered nerves, as well as further revealing the relationship between angiogenesis and nerve regeneration.

As experimental techniques advance, more comprehensive and objective imaging methods for visualizing angiogenesis in tissue-engineered nerves will appear. However, blood vessel three-dimensional reconstruction using MICROFIL perfusion and micro-CT scanning is currently a good method for visualizing newly formed blood vessels in tissue-engineered nerves implanted *in vivo* and provides an experimental basis for further research on nerve regeneration.

Author contributions: *XSG checked and revised this article. YMY participated in study concept. HKW designed and performed experiments, and wrote the paper. YXW designed and performed the experiments, and collected data. CBX, ZMYL, JH and YHZ performed experiments. All authors approved the final version of the paper.*

Conflicts of interest: *None declared.*

Plagiarism check: *This paper was screened twice using Cross-Check to verify originality before publication.*

Peer review: *This paper was double-blinded and stringently reviewed by international expert reviewers.*

References

Barbetta A, Bedini R, Pecci R, Dentini M (2012) Role of X-ray microtomography in tissue engineering. Ann Ist Super Sanita 48:10-18.

Biernaskie JA, McKenzie IA, Toma JG, Miller FD (2006) Isolation of skin-derived precursors (SKPs) and differentiation and enrichment of their Schwann cell progeny. Nat Protoc 1:2803-2812.

Carmeliet P, Jain RK (2011) Molecular mechanisms and clinical applications of angiogenesis. Nature 473:298-307.

Cheung LK (1996) The blood supply of the human temporalis muscle: a vascular corrosion cast study. J Anat 189:431-438.
Dew L, MacNeil S, Chong CK (2015) Vascularization strategies for tissue engineers. Regen Med 10:211-224.
Garcia-Sanz A, Rodriguez-Barbero A, Bentley MD, Ritman EL, Romero JC (1998) Three-dimensional microcomputed tomography of renal vasculature in rats. Hypertension 31:440-444.
Goerke SM, Obermeyer J, Plaha J, Stark GB, Finkenzeller G (2015) Endothelial progenitor cells from peripheral blood support bone regeneration by provoking an angiogenic response. Microvasc Res 98:40-47.
Gu Y, Zhu J, Xue C, Li Z, Ding F, Yang Y, Gu X (2014) Chitosan/silk fibroin-based, Schwann cell-derived extracellular matrix-modified scaffolds for bridging rat sciatic nerve gaps. Biomaterials 35:2253-2263.
Hasan MR, Herz J, Hermann DM, Doeppner TR (2013) Intravascular perfusion of carbon black ink allows reliable visualization of cerebral vessels. J Vis Exp:pii: 4374.
Hu N, Wu H, Xue C, Gong Y, Wu J, Xiao Z, Yang Y, Ding F, Gu X (2013) Long-term outcome of the repair of 50 mm long median nerve defects in rhesus monkeys with marrow mesenchymal stem cells-containing, chitosan-based tissue engineered nerve grafts. Biomaterials 34:100-111.
Jiang X, Xiong Q, Xu G, Lin H, Fang X, Cui D, Xu M, Chen F, Geng H (2015) VEGF-loaded nanoparticle-modified BAMAs enhance angiogenesis and inhibit graft shrinkage in tissue-engineered bladder. Ann Biomed Eng doi: 10.1007/s10439-015-1284-9.
Jin XL, Zheng Y, Shen HM, Jing WL, Zhang ZQ, Huang JZ, Tan QL (2005) Analysis of the mechanisms of rabbit's brainstem hemorrhage complicated with irritable changes in the alvine mucous membrane. World J Gastroenterol 11:1610-1615.
Jing XL, Farberg AS, Monson LA, Donneys A, Tchanque-Fossuo CN, Buchman SR (2012) Radiomorphometric quantitative analysis of vasculature utilizing micro-computed tomography and vessel perfusion in the murine mandible. Craniomaxillofac Trauma Reconstr 5:223-230.
Kanzaki H, Okamura H, Okuda Y, Takenaka A, Morimoto K, Nishimura T (1982) Scanning electron microscopic study of rabbit ovarian follicle microvasculature using resin injection-corrosion casts. J Anat 134:697-704.
Kline TL, Knudsen BE, Anderson JL, Vercnocke AJ, Jorgensen SM, Ritman EL (2014) Anatomy of hepatic arteriolo-portal venular shunts evaluated by 3D micro-CT imaging. J Anat 224:724-731.
Lee S, Barbe MF, Scalia R, Goldfinger LE (2014) Three-dimensional reconstruction of neovasculature in solid tumors and basement membrane matrix using ex vivo X-ray micro-computed tomography. Microcirculation 21:159-170.
Li S, Wang X, Gu Y, Chen C, Wang Y, Liu J, Hu W, Yu B, Wang Y, Ding F, Liu Y, Gu X (2015) Let-7 microRNAs regenerate peripheral nerve regeneration by targeting nerve growth factor. Mol Ther 23:423-433.
Liu X, Terry T, Pan S, Yang Z, Willerson JT, Dixon RAF, Liu Q (2013) Osmotic drug delivery to ischemic hindlimbs and perfusion of vasculature with microfil for micro-computed tomography imaging. J Vis Exp:e50364.
Marinković D, Kukolj V, Aleksić-Kovačević S, Jovanović M, Knežević M (2013) The role of hepatic myofibroblasts in liver cirrhosis in fallow deer (Dama dama) naturally infected with giant liver fluke (Fascioloides magna). BMC Vet Res 9:45.
Nyangoga H, Mercier P, Libouban H, Baslé MF, Chappard D (2011) Three-dimensional characterization of the vascular bed in bone metastasis of the rat by microcomputed tomography (MicroCT). PLoS One 6:e17336.
Osborn SL, So M, Hambro S, Nolta JA, Kurzrock EA (2015) Inosculation of blood vessels allows early perfusion and vitality of bladder grafts-implications for bioengineered bladder wall. Tissue Eng Part A 21:1906-1915.
Oxlund BS, Ørtoft G, Brüel A, Danielsen CC, Bor P, Oxlund H, Uldbjerg N (2010) Collagen concentration and biomechanical properties of samples from the lower uterine cervix in relation to age and parity in non-pregnant women. Reprod Biol Endocrinol 8:82.
Potente M, Gerhardt H, Carmeliet P (2011) Basic and therapeutic aspects of angiogenesis. Cell 146:873-887.
Savransky V, Sanford DC, Syar E, Austin JL, Tordoff KP, Anderson MS, Stark GV, Barnewall RE, Briscoe CM, Lemiale-Biérinx L, Park S, Ionin B, Skiadopoulos MH (2013) Pathology and pathophysiology of inhalational anthrax in a guinea pig model. Infect Immun 81:1152-1163.
Shafiq M, Jung Y, Kim SH (2015) Stem cell recruitment, angiogenesis, and tissue regeneration in substance P-conjugated poly(l-lactide-co-ε-caprolactone) nonwoven meshes. J Biomed Mater Res A 103:2673-2688.
Toma JG, Akhavan M, Fernandes KJ, Barnabé-Heider F, Sadikot A, Kaplan DR, Miller FD (2001) Isolation of multipotent adult stem cells from the dermis of mammalian skin. Nat Cell Biol 3:778-784.
Unger RE, Dohle E, Kirkpatrick CJ (2015) Improving vascularization of engineered bone through the generation of pro-angiogenic effects in co-culture systems. Adv Drug Deliver Rev doi:10.1016/j.addr.2015.03.012.
Walter TJ, Sparks EE, Huppert SS (2012) 3-dimensional resin casting and imaging of mouse portal vein or intrahepatic bile duct system. J Vis Exp:e4272.
Wang H, Zhao Q, Zhao W, Liu Q, Gu X, Yang Y (2012) Repairing rat sciatic nerve injury by a nerve-growth-factor-loaded, chitosan-based nerve conduit. Biotechnol Appl Biochem 59:388-394.
Wang L, Zhang B, Bao C, Habibovic P, Hu J, Zhang X (2014a) Ectopic osteoid and bone formation by three calcium-phosphate ceramics in rats, rabbits and dogs. PLoS One 9:e107044.
Wang X, Hu W, Cao Y, Yao J, Wu J, Gu X (2005) Dog sciatic nerve regeneration across a 30-mm defect bridged by a chitosan/PGA artificial nerve graft. Brain 128:1897-1910.
Wang Y, Zhao Y, Sun C, Hu W, Zhao J, Li G, Zhang L, Liu M, Liu Y, Ding F, Yang Y, Gu X (2014b) Chitosan degradation products promote nerve regeneration by stimulating schwann cell proliferation via miR-27a/FOXO1 axis. Mol Neurobiol doi:10.1007/s12035-014-8968-2:1-12.
Wang ZK, Shi H, Wang SD, Liu J, Zhu WM, Yang MF, Liu C, Lu H, Wang FY (2014c) Confusing untypical intestinal Behcet's disease: skip ulcers with severe lower gastrointestinal hemorrhage. World J Gastrointest Endosc 6:27-31.
Xue S, Gong H, Jiang T, Luo W, Meng Y, Liu Q, Chen S, Li A (2014) Indian-ink perfusion based method for reconstructing continuous vascular networks in whole mouse brain. PLoS One 9:e88067.
Yang Y, Yuan X, Ding F, Yao D, Gu Y, Liu J, Gu X (2011) Repair of rat sciatic nerve gap by a silk fibroin-based scaffold added with bone marrow mesenchymal stem cells. Tissue Eng Part A 17:2231-2244.
Zhou S, Zhang S, Wang Y, Yi S, Zhao L, Tang X, Yu B, Gu X, Ding F (2015) miR-21 and miR-222 inhibit apoptosis of adult dorsal root ganglion neurons by repressing TIMP3 following sciatic nerve injury. Neurosci Lett 586:43-49.

Copyedited by McCarty W, Norman C, Yu J, Qiu Y, Li CH, Song LP, Zhao M